ChemComm

COMMUNICATION

View Article Online
View Journal | View Issue

Cite this: *Chem. Commun.*, 2022, **58**, 10695

Received 28th July 2022,
Accepted 30th August 2022

DOI: 10.1039/d2cc04209f

rsc.li/chemcomm

Triple helix and rod structures of the antiseptic drug bibrocathol revealed by electron crystallography†

Erik Svensson Grape,* Tom Willhammar and A. Ken Inge

Bibrocathol is an active pharmaceutical ingredient that has been used to treat eyelid diseases for over a century, yet its structure has remained unknown. 3D electron diffraction on crystals from a commercial ointment revealed two structures. These results highlight the technique's potential in structure elucidation from microcrystalline mixtures.

Determining the structures of pharmaceutical compounds is of great importance, both in terms of functional and mechanistic insight, but also for validation and intellectual property claims. The existence of multiple structures of a chemical substance or analogues, such as solvates, may also greatly influence properties such as the stability, solubility and bioavailability of an active pharmaceutical ingredient (API). While the standard method for structure determination of crystalline materials is single-crystal X-ray diffraction (SCXRD), the requirement of large, well-diffracting crystals is a significant limitation of the technique, as many compounds can only be acquired as small submicrometer-sized crystals. Additionally, the coexistence of multiple phases in a mixture may further complicate characterization and structure determination by techniques such as powder X-ray diffraction (PXRD).

3D electron diffraction (3D ED) techniques have emerged as an alternative method of structure determination,[1–4] facilitating data collection from submicrometer crystals. 3D ED has been used to determine structures of pure molecular compounds, as well as complex pharmaceutical formulations.[3,5–10] The technique has also been applied in the investigation of long-known polymorphs that were previously challenging to characterize.[11] Additionally, proof-of-concept studies have demonstrated that structures of APIs could be directly determined from small crystallites obtained from commercially available pills.[7,12]

While the large majority of APIs are organic molecules, metallodrugs are found at the crossroads of pharmaceutical and inorganic compounds, being pharmaceutical formulations where a metal or metal cation is part of the API.[13] One notable class of metallodrugs are those containing bismuth, which are largely used for their antimicrobial properties in the treatment of gastrointestinal disorders, such as *H. pylori* infections and gastric ulcers. Bismuth-based formulations have also shown promise in treating infections of viruses and multidrug-resistant bacterial strains.[14,15] All the while, compounds of bismuth tend to be difficult to acquire as large single crystals, making their structural characterization a significant challenge.[16–18] As such, the use of 3D ED has proven particularly valuable for determining the structure of these compounds, including bismuth subgallate[19] and bismuth subsalicylate[20] (the active ingredient of Pepto-Bismol).

Bibrocathol (Fig. 1), also known as tetrabromopyrocatechol bismuth, is the active ingredient of over-the-counter topical ointments sold under brand names such as Noviform® and Posiformin®, and is commonly used to treat eyelid infections and inflammation such as blepharitis.[21,22] It is a crystalline substance, yet no crystal structure has previously been reported.

Investigations of bismuth subgallate and bismuth subsalicylate by 3D ED showed that these compounds were in fact coordination polymers, with extended 1D or 2D structures, rather than isolated metal complexes, as they have been commonly depicted in molecular sketch diagrams. This begs the question of what the actual structure of bibrocathol is. In this work we show that

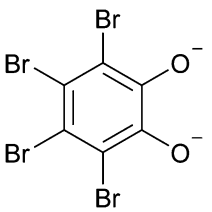

Fig. 1 Molecular structure of a fully deprotonated tetrabromocatecholate dianion, which, together with Bi^{3+}, are constituents of the active pharmaceutical ingredient bibrocathol.

Department of Materials and Environmental Chemistry, Stockholm University, SE-106 91, Stockholm, Sweden. E-mail: erik.grape@mmk.su.se

† Electronic supplementary information (ESI) available. CCDC 2190211 and 2190212. For ESI and crystallographic data in CIF or other electronic format see DOI: https://doi.org/10.1039/d2cc04209f

the formulation is a mixture of two crystalline phases, both of which are indeed extended structures.

For 3D ED data collection, over-the-counter Noviform® (5% bibrocathol in a mixture of inactive ingredients: Vaseline, liquid paraffin, cetostearyl alcohol and lanolin) was purchased from a local pharmacy. The as-bought yellow ointment was washed with toluene to remove the greasy amorphous inactive ingredients. PXRD patterns were recorded before and after washing (Fig. S1, ESI†), and indicate that the yellow crystalline powder was unaffected by the washing process. The isolated powder was used for 3D ED measurements at room temperature by sprinkling the powder over holey carbon TEM grids (see ESI† for experimental details).

In the transmission electron microscope (TEM), rod-shaped crystals of two distinct morphologies could be observed (Fig. 2a and b) and 3D ED datasets from multiple crystals of both morphologies were collected. All in all, a total of 5 datasets could be indexed to a monoclinic unit cell (a = 17.01 Å, b = 27.26 Å, c = 26.21 Å, β = 94.7°) and a total of 7 datasets could be indexed to a tetragonal unit cell (a = 25.16 Å, c = 13.98 Å). As is evident in Fig. 2, the tetragonal rod-shaped crystals have sharp facets perpendicular to the length-wise direction (Fig. 2b), in contrast to the monoclinic crystals which have rounded ends (Fig. 2a). Even so, the phases are not always easy to distinguish in the TEM as they tend exist in aggregates (Fig. S4, ESI†) and the difference in morphology is rather minor. The reconstructed reciprocal lattice of the 3D ED datasets collected on both phases show well-resolved reflections (Fig. 2c and d). Datasets of each phase were integrated using the aforementioned unit cells and exhibited reflection conditions consistent with the space groups $P2_1/n$ and $I4_1/a$ for the monoclinic and tetragonal phases, respectively (see Table S2, ESI† for full list of refinement statistics of the merged datasets). After integration, the structures of both phases could be solved, successfully locating all the non-hydrogen atoms in the initial structure solution, and revealing that both phases consist of packings of extended 1-periodic coordination polymers (Fig. 3). Notably, the monoclinic phase (Fig. 3a–c) is rather complicated, consisting of 10 bismuth cations, 5 oxide anions, and 10 tetrabromocatecholate anions, adding up to a total of 135 unique non-hydrogen atoms in the asymmetric unit of the crystal structure ($C_{60}Bi_{10}Br_{40}O_{25}$).

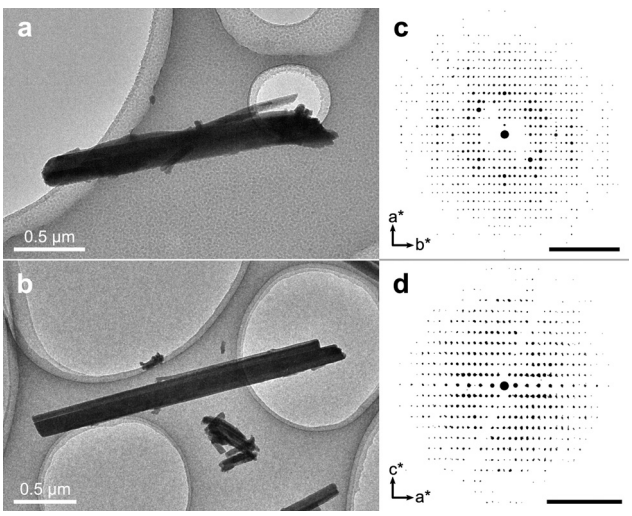

Fig. 2 Transmission electron microscopy images of representative bibrocathol crystals of the (a) monoclinic phase and (b) the tetragonal phase. Reconstructed reciprocal lattice of individual datasets of (c) the monoclinic and (d) the tetragonal phase. Black scale bars are equal to 0.5 $Å^{-1}$.

Determination of such a complicated structure amongst a mixture of multiple unknown phases using techniques such as PXRD, would have been rather unfeasible. In fact, to the best of our knowledge, the structure of this dominant monoclinic phase is currently the third[23,24] most complicated structure determined by electron diffraction so far, based on current electron diffraction entries in the CSD.[25] The triple helix in the monoclinic phase has a formula of $[Bi_2O(C_6Br_4O_2)_2]_n$. The central core of the helix is made of μ_4-O^{2-} anions and Bi^{3+} cations. The TBC^{2-} anions surround the core with the bromine atoms on the outer surface of the helix. The Bi^{3+} cations have a coordination number of either 6 or 7. The Bi–O distances found within the structure range between 2.1 and 3.1 Å, and each Bi^{3+} cation has a hemidirected coordination environment, *i.e.* a hemisphere of its coordination sphere is essentially unoccupied due to the stereochemically active 6s lone pair electrons on the Bi^{3+} cation. The catecholate groups of all TBC^{2-} anions in the structure each chelate to Bi^{3+} cations and simultaneously bridge neighbouring Bi^{3+} cations along the helix. Neighbouring TBC^{2-} anions along the helix are stacked and are nearly co-planar with a slight skew. These closely stacked TBC^{2-} ligands follow a helical path, and three such helices of TBC^{2-} ligands surround the central bismuth-oxo core, resulting in the triple helix. One full turn of the triple helix has a repeating period of 82 Å, which is three times the length of the crystallographic b axis (Fig. 3c), *i.e.* one unit cell comprised of a 1/3 turn of the triple helix (Fig. 3d).

The tetragonal phase consists of rods, and from a crystallographic perspective the structure is significantly simpler to describe as the asymmetric unit consists of just 26 non-hydrogen atoms. The rods are of Bi^{3+} cations that are chelated by the catecholate groups of two TBC^- anions and the coordination sphere is completed by the presence of two bridging catecholate oxygens of neighbouring TBC^- anions in the structure.

The coordination number of the single Bi^{3+} cation in the tetragonal structure is 6, with Bi–O distances found in the range of 2.1 to 2.8 Å. Additionally, a non-coordinated oxygen atom, attributed to a water molecule, could be found in the structure. This oxygen atom occupies a pocket between what is presumed to be partially protonated TBC^- anions in the rod-like structure. This water molecule forms strong hydrogen bonds to the adjacent oxygens of TBC^- anions, likely further enforced by the pocket in which the water molecule sits, with donor–acceptor distances of approximately 2.4 Å, where strong and largely covalent hydrogen-bonding interactions typically fall in the donor–acceptor distance range of 2.2–2.5 Å.[26] The proposed formula of $[Bi(C_6Br_4O_2)(C_6Br_4OOH)\cdot H_2O]_n$ for the tetragonal phase, where one catecholate oxygen remains protonated, would give a charge-balanced material with a bismuth to bromine ratio of 1 : 8.

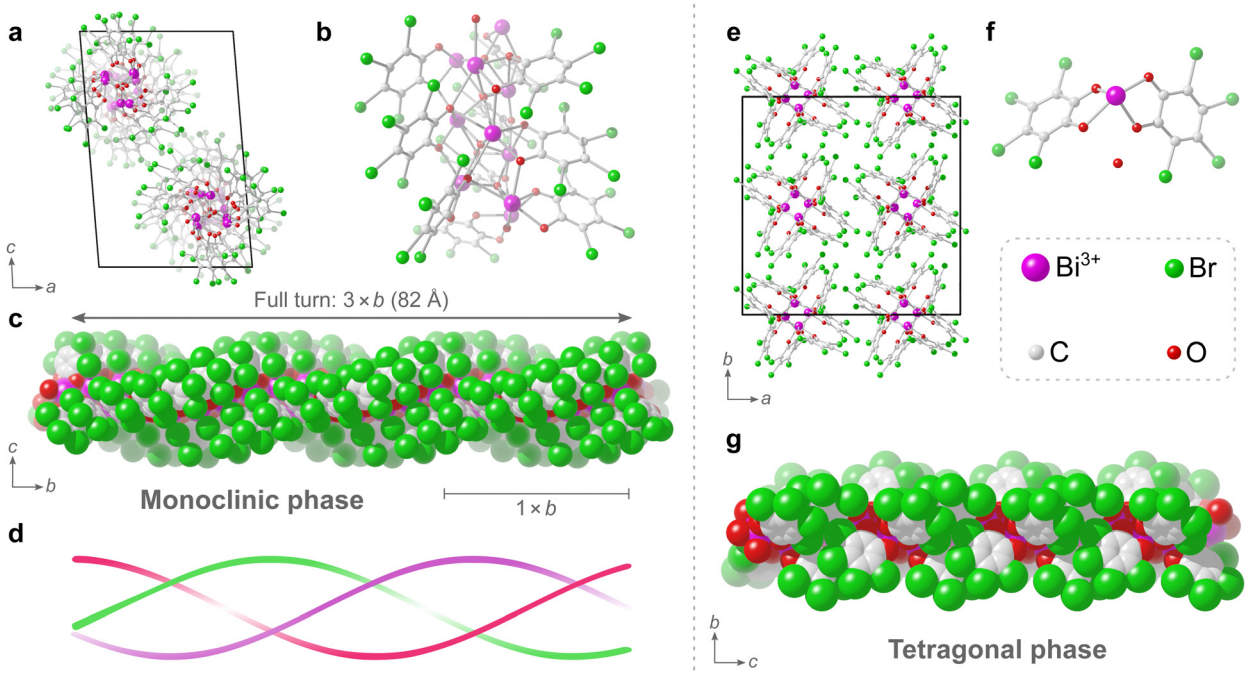

Fig. 3 (a) Structure of the monoclinic bibrocathol phase as viewed along *b*, where two helices of opposite handedness are illustrated inside the unit cell (black edges). (b) Asymmetric unit of the monoclinic structure, comprised by a total of 135 unique atoms. (c) The helical structure of the monoclinic phase drawn in a space-filling representation and viewed along *a*, where the rotation period of the helix is 82 Å (3 × *b*). (d) A schematic representation of the triple helix present in the monoclinic structure. (e) Structure of the tetragonal bibrocathol phase as viewed along *c*, showing a packing of the rods. Hydrogen atoms are omitted for clarity. (f) Asymmetric unit of the tetragonal phase. (g) Side view of the rod in the tetragonal phase, drawn in a space-filling representation, as viewed along *a*.

Analysing the bulk of the washed solid with elemental analysis (Table S3, ESI†) and PXRD indicates the helical monoclinic phase as the predominant phase in the washed solid. Elemental analysis showed a bismuth to bromine atomic ratio of 1 : 4, where the expected values are 1 : 4 and 1 : 8 for the monoclinic and tetragonal phases, respectively. In addition, the experimental PXRD pattern has significantly higher intensity peaks at positions expected for the monoclinic phase rather than the tetragonal phase (Fig. S2, ESI†). The observed changes in unit cell parameters are likely related to a slight shift in the packing of the helical or rod-like units upon exposure to the low-pressure environment of the TEM, as the most significant changes are observed in the basal plane perpendicular to the rod direction, *i.e.* the *ac* and *ab* planes for the monoclinic and tetragonal phase, respectively. Variable temperature PXRD measurements showed little to no changes upon exposure to reduced pressure, even at higher temperatures (Fig. S3, ESI†).

In summary, a commercial formulation (Noviform 5%) of the active pharmaceutical ingredient bibrocathol was analysed, revealing the structures of this crystalline pharmaceutical. The measurements showed that the formulation is a mixture of two distinct phases of different compositions, where the complex and dominant monoclinic phase with a formula of $[Bi_2O(C_6Br_4O_2)_2]_n$ is one of the more intricate structures solved by 3D ED so far, having 135 crystallographically unique atoms in the asymmetric unit. This work highlights the potential of using 3D ED as a stand-alone technique for determining the structures of active pharmaceutical ingredients from mixtures. Further, this work showcases the possibility of performing detailed structural characterization of crystalline solids using 3D ED, acquiring atomically precise structures from complex microcrystalline phase mixtures found in commercially available samples.

This work was supported by the Swedish Foundation for Strategic Research (SSF, ICA-7) and the Swedish Research Council (VR, 2019-05465). The authors thank Prof. Dr. Werner Winter for insightful correspondence that inspired the start of this investigation.

Conflicts of interest

There are no conflicts to declare.

Notes and references

1 I. Nederlof, E. van Genderen, Y.-W. Li and J. P. Abrahams, *Acta Crystallogr., Sect. D: Biol. Crystallogr.*, 2013, **69**, 1223–1230.
2 L. Palatinus, P. Brázda, P. Boullay, O. Perez, M. Klementová, S. Petit, V. Eigner, M. Zaarour and S. Mintova, *Science*, 2017, **355**, 166–169.
3 C. G. Jones, M. W. Martynowycz, J. Hattne, T. J. Fulton, B. M. Stoltz, J. A. Rodriguez, H. M. Nelson and T. Gonen, *ACS Cent. Sci.*, 2018, **4**, 1587–1592.
4 M. Gemmi, E. Mugnaioli, T. E. Gorelik, U. Kolb, L. Palatinus, P. Boullay, S. Hovmöller and J. P. Abrahams, *ACS Cent. Sci.*, 2019, **5**, 1315–1329.
5 T. E. Gorelik, J. Van De Streek, A. F. M. Kilbinger, G. Brunklaus and U. Kolb, *Acta Crystallogr., Sect. B: Struct. Sci.*, 2012, **68**, 171–181.

6 E. Van Genderen, M. T. B. Clabbers, P. P. Das, A. Stewart, I. Nederlof, K. C. Barentsen, Q. Portillo, N. S. Pannu, S. Nicolopoulos, T. Gruene and J. P. Abrahams, *Acta Crystallogr., Sect. A: Found. Adv.*, 2016, **72**, 236–242.
7 T. Gruene, J. T. C. Wennmacher, C. Zaubitzer, J. J. Holstein, J. Heidler, A. Fecteau-Lefebvre, S. De Carlo, E. Müller, K. N. Goldie, I. Regeni, T. Li, G. Santiso-Quinones, G. Steinfeld, S. Handschin, E. van Genderen, J. A. van Bokhoven, G. H. Clever and R. Pantelic, *Angew. Chem., Int. Ed.*, 2018, **57**, 16313–16317.
8 P. Brázda, L. Palatinus and M. Babor, *Science*, 2019, **364**, 667–669.
9 I. Andrusenko, V. Hamilton, E. Mugnaioli, A. Lanza, C. Hall, J. Potticary, S. R. Hall and M. Gemmi, *Angew. Chem., Int. Ed.*, 2019, **58**, 10919–10922.
10 G. R. Woollam, P. P. Das, E. Mugnaioli, I. Andrusenko, A. S. Galanis, J. Van De Streek, S. Nicolopoulos, M. Gemmi and T. Wagner, *CrystEngComm*, 2020, **22**, 7490–7499.
11 M. Lightowler, S. Li, X. Ou, X. Zou, M. Lu and H. Xu, *Angew. Chem., Int. Ed.*, 2022, **61**, e202114985.
12 C. G. Jones, M. W. Martynowycz, J. Hattne, T. J. Fulton, B. M. Stoltz, J. A. Rodriguez, H. M. Nelson and T. Gonen, *ACS Cent. Sci.*, 2018, **4**, 1587–1592.
13 E. J. Anthony, E. M. Bolitho, H. E. Bridgewater, O. W. L. Carter, J. M. Donnelly, C. Imberti, E. C. Lant, F. Lermyte, R. J. Needham, M. Palau, P. J. Sadler, H. Shi, F. X. Wang, W. Y. Zhang and Z. Zhang, *Chem. Sci.*, 2020, **11**, 12888–12917.
14 R. Wang, T. P. Lai, P. Gao, H. Zhang, P. L. Ho, P. C. Y. Woo, G. Ma, R. Y. T. Kao, H. Li and H. Sun, *Nat. Commun.*, 2018, **9**, 439.
15 D. M. Griffith, H. Li, M. V. Werrett, P. C. Andrews and H. Sun, *Chem. Soc. Rev.*, 2021, **50**, 12037–12069.
16 J. H. Thurston, E. M. Marlier and K. H. Whitmire, *Chem. Commun.*, 2002, 2384–2835.
17 P. C. Andrews, G. B. Deacon, C. M. Forsyth, P. C. Junk, I. Kumar and M. Maguire, *Angew. Chem., Int. Ed.*, 2006, **45**, 5638–5642.
18 V. André, A. Hardeman, I. Halasz, R. S. Stein, G. J. Jackson, D. G. Reid, M. J. Duer, C. Curfs, M. T. Duarte and T. Friščić, *Angew. Chem., Int. Ed.*, 2011, **50**, 7858–7861.
19 Y. Wang, S. Takki, O. Cheung, H. Xu, W. Wan, L. Öhrström and A. K. Inge, *Chem. Commun.*, 2017, **53**, 7018–7021.
20 E. Svensson Grape, V. Rooth, M. Nero, T. Willhammar and A. K. Inge, *Nat. Commun.*, 2022, **13**, 1984.
21 W. Behrens-Baumann, C. Niederdellmann, A. Jehkul and R. Kohnen, *Ophthalmologe*, 2006, **103**, 960–965.
22 P. A. Bezdetko, N. Sergienko, Y. Dyomin, A. Korol, N. Nikitin, M. Merzbacher, D. Groß and R. Kohnen, *Graefes Arch. Clin. Exp. Ophthalmol.*, 2012, **250**, 1869–1875.
23 S. Vergara, D. A. Lukes, M. W. Martynowycz, U. Santiago, G. Plascencia-Villa, S. C. Weiss, M. J. De La Cruz, D. M. Black, M. M. Alvarez, X. López-Lozano, C. O. Barnes, G. Lin, H. C. Weissker, R. L. Whetten, T. Gonen, M. J. Yacaman and G. Calero, *J. Phys. Chem. Lett.*, 2017, **8**, 5523–5530.
24 K. Kato, K. Takaba, S. Maki-Yonekura, N. Mitoma, Y. Nakanishi, T. Nishihara, T. Hatakeyama, T. Kawada, Y. Hijikata, J. Pirillo, L. T. Scott, K. Yonekura, Y. Segawa and K. Itami, *J. Am. Chem. Soc.*, 2021, **143**, 5465–5469.
25 C. R. Groom, I. J. Bruno, M. P. Lightfoot and S. C. Ward, *Acta Crystallogr.*, 2016, **B72**, 171–179.
26 G. Desiraju and T. Steiner, *The Weak Hydrogen Bond*, Oxford University Press, 1st edn, 1999, pp. 14–16.

